Astrophysics and Space Science (2024) 369:39
https://doi.org/10.1007/s10509-024-04303-9

RESEARCH

Thrust continuation of time-optimal orbital transfers with soft terminal conditions

Yang Wang[1] · Xiyun Hou[1] · Francesco Topputo[2]

Received: 4 March 2024 / Accepted: 5 April 2024

Abstract
Time-optimal orbital transfers with soft terminal conditions are studied in this work. First, a two-layer thrust continuation method is devised. The unfavorable thrust continuation path is handled by switching between different solution curves. Second, the proposed method is applied to solving time-optimal transfers under two- or three-body dynamics with Cartesian coordinates to verify its effectiveness. The near conservation of the product between the time of flight and the thrust level is observed for general orbital transfers. A linear variation of this quantity with eccentricity is also illustrated when the difference in eccentricity between the initial and terminal orbits is large enough.

Keywords Low thrust · Thrust continuation · Many-revolution transfers

1 Introduction

Increasing attention has been paid on low-thrust propulsion in recent decades due to its higher fuel efficiency compared to chemical propulsion. The low level of the thrust produces trajectories encompassing many revolutions before reaching the desired orbit. The corresponding nonlinear optimal control problem (NOCP) is challenging, since the sensitivity to the initial guess amplifies as the number of revolutions grows (Aziz et al. 2018).

Optimal control methods dedicated to solving optimal low-thrust trajectories are mainly categorized as direct and indirect methods. Direct methods transform the NOCP to a finite-dimensional nonlinear programming problem (NLP), and then a solution fulfilling the Karush-Kuhn-Tucker conditions is sought (Topputo and Zhang 2014). Direct methods can handle complicated constraints with a broad convergence domain, yet a large number of variables are usually required to obtain accurate many-revolution trajectories (Topputo and Zhang 2014). Alternatively, indirect methods transform the NOCP to a two-point boundary value problem, then solve it as a zero-finding problem (Conway 2012). Solutions from indirect methods are guaranteed to satisfy first-order necessary conditions of optimality, but guessing unknown costates is nonintuitive due to the lack of their physical interpretation (Conway 2012).

To effectively expand the convergence domain of indirect methods, homotopy continuation methods have been widely used in low-thrust trajectory optimization (Bertrand and Epenoy 2002; Chi et al. 2017; Pan et al. 2018; Li et al. 2021; Wang and Topputo 2023). Instead of attacking the original problem directly, homotopy continuation methods gradually approach the solution of the original problem by tracking the homotopy path, which is comprised of a series of auxiliary problems (Allgower and Georg 2003). Thrust continuation approaches the solution by gradually reducing the thrust level to the desired value, which is studied in this work because: 1) it provides an easier way to search for a difficult many-revolution solution; 2) it provides information about how the solution varies as the thrust level varies.

However, thrust continuation may encounter unfavorable conditions, involving limit points where the path terminates when monotonously varying the thrust level, or the path goes off to infinity (Pan et al. 2016). The pseudo-arclength method (PAM) can effectively pass limit points and then

✉ Y. Wang
yang.wang@nju.edu.cn

X. Hou
houxiyun@nju.edu.cn

F. Topputo
francesco.topputo@polimi.it

[1] School of Astronomy and Space Science, Nanjing University, Xianlin Avenue 163, Nanjing, 210023, China

[2] Department of Aerospace Science and Technology, Politecnico di Milano, Via La Masa 34, Milan, 20156, Italy

Published online: 12 April 2024

track the homotopy path that reverses the path direction (Wang and Topputo 2022). In Pan et al. (2016), a two-layer continuation method was developed to handle unfavorable conditions by tracking a discontinuous path. In Pan et al. (2020, 2018), PAM was used to tackle limit points, and the homotopy function was designed to find time-optimal transfers. However, continuation procedures in Pan et al. (2020, 2018, 2016) lack physical interpretation. In Caillau and Farrés (2016), the continuation on the angle that defines the geostationary orbit (GEO) under the Earth-Moon Circular Restricted Three-Body Problem (CRTBP) was executed to search multiple time-optimal GEO-L1 trajectories with the same thrust level. In Ferella (2016), a two-layer thrust continuation was designed to solve time-optimal geostationary transfer orbit (GTO) to GEO transfers. The unfavorable conditions were addressed by switching solution curves, achieved by leveraging the true anomaly as the continuation parameter in the second-layer continuation. The longitude-thrust-homotopy was used in Zhang et al. (2023) to study the global solution space of time-optimal GTO-GEO transfers.

The continuation of the physical angle has the following benefits: 1) it can be used to tackle unfavorable conditions of thrust continuation by switching solution curves; 2) the continuation procedure has more physical significance. For fixed-point terminal constraints, the difference between neighborhood local solutions with the same thrust level in the true anomaly is 2π, which is common for different transfer problems. This fact can be used as the stop condition when searching for the neighborhood solution by continuing from the current solution. For soft terminal conditions where the terminal state of the spacecraft is required to satisfy a set of functional constraints, it is desirable to find the common stop condition to simplify the algorithm complexity. Additionally, current methods were designed specifically for either two-body or CRTBP dynamics. It is necessary to develop a method that can be commonly used for different dynamics with soft terminal conditions.

Based on time-optimal solutions on the thrust continuation path, the near constant of the product of the transfer time and the thrust level was observed for GTO-GEO transfers (Caillau et al. 2003; Taheri 2021; Zhang et al. 2023). This empirical result was also illustrated in intercept and rendezvous transfers, and it was found that this relationship does not hold for high-thrust ranges (Yue et al. 2010). The further study in Zhang et al. (2023) concluded that the empirical result holds for the constant in a range of values. A theoretical explanation of this empirical result was provided in Bonnard and Caillau (2009). Although the near conservation was observed for GTO-GEO transfers, it is still not clear the relationship between this quantity with terminal conditions.

This work presents a simple two-layer thrust continuation method to solve time-optimal low-thrust trajectories with soft terminal conditions. When the thrust continuation fails to proceed, the second-layer continuation is triggered to search for solutions with the same thrust level but different revolutions. The key is to augment the state by adding an auxiliary angle that defines the revolution. The dynamic of the auxiliary angle does not involve control variables. Also, the corresponding costate is constant along the transfer. These facts allow for defining suitable auxiliary problems for the second-layer continuation. The features of our method are that 1) it can be applied to both two- and multi-body dynamics; 2) the stop condition when the neighborhood solution is reached by continuing from the current solution can be commonly used for different transfer problems. Extensive simulations from GTO to GEO, Elliptic Inclined Geosynchronous Orbit (EIGSO), and Halo orbit under Cartesian coordinates are carried out. The conservation of the product of the transfer time and the thrust level for general transfer problems is observed and discussed.

The rest of this paper is organized as follows. Section 2 states the time-optimal many-revolution problem. Section 3 depicts the developed method. Section 4 presents numerical simulations. Section 5 concludes this paper.

2 Time-optimal transfers

The equations of motion for the spacecraft under Cartesian coordinates are

$$\dot{\boldsymbol{x}} = \boldsymbol{f}(\boldsymbol{x}, u, \boldsymbol{\alpha}) \Rightarrow \begin{cases} \dot{\boldsymbol{r}} = \boldsymbol{v} \\ \dot{\boldsymbol{v}} = \boldsymbol{g}(\boldsymbol{r}) + \boldsymbol{h}(\boldsymbol{v}) + u\dfrac{T_{\max}}{m}\boldsymbol{\alpha} \\ \dot{m} = -u\dfrac{T_{\max}}{I_{\text{sp}}\, g_0} \end{cases} \tag{1}$$

where $\boldsymbol{r} = [x, y, z]$, $\boldsymbol{v} = [v_x, v_y, v_z]$, and m are the position vector, the velocity vector, and the mass, respectively; $\boldsymbol{x} := [\boldsymbol{r}, \boldsymbol{v}, m]$ is the state vector, $u \in [0, 1]$ is the thrust throttle factor, $\boldsymbol{\alpha}$ is the thrust direction unit vector, and g_0 is the gravitational acceleration at sea level; $\boldsymbol{g}(\boldsymbol{r})$ and $\boldsymbol{h}(\boldsymbol{v})$ are vector-value functions of $\boldsymbol{r}$ and $\boldsymbol{v}$, respectively. Both the maximum thrust $T_{\max}$ and the specific impulse I_{sp} are assumed constant.

The transfer time, fuel consumption, and their combination are the main indices to be minimized in the trajectory design (Coverstone-Carroll et al. 2000; Niccolai 2024). The solution of the time-optimal problem provides the minimum time required to achieve the transfer. The developed method in this work is designed for the time-optimal problem. The

performance index of the time-optimal problem is

$$J = \int_{t_i}^{t_f} 1 \, \mathrm{d}t \tag{2}$$

where t_i and t_f are the initial and terminal time, respectively.

The Hamiltonian function associated to the time-optimal problem is

$$H = 1 + \boldsymbol{\lambda}_r^\top \boldsymbol{v} + \boldsymbol{\lambda}_v^\top \left(\boldsymbol{g}(\boldsymbol{r}) + \boldsymbol{h}(\boldsymbol{v}) + u \, \frac{T_{\max}}{m} \boldsymbol{\alpha} \right) - \lambda_m u \frac{T_{\max}}{I_{\mathrm{sp}} \, g_0} \tag{3}$$

where $\boldsymbol{\lambda} := [\boldsymbol{\lambda}_r, \boldsymbol{\lambda}_v, \lambda_m]$ is the costate vector associated to $\boldsymbol{x}$. The equation of costate dynamics is

$$\dot{\boldsymbol{\lambda}} = -\left(\frac{\partial H(\boldsymbol{x}, \boldsymbol{\lambda}, u, \boldsymbol{\alpha})}{\partial \boldsymbol{x}} \right)^\top \tag{4}$$

By virtue of the Pontryagin minimum principle (Bryson and Ho 1975), the optimal thrust direction $\boldsymbol{\alpha}^*$ satisfies

$$\boldsymbol{\alpha}^* = -\frac{\boldsymbol{\lambda}_v}{\lambda_v} \tag{5}$$

and the optimal thrust throttle factor u^* is

$$u^* = \begin{cases} 1 & S < 0 \\ 0 & S > 0 \\ (0, 1) & S = 0 \end{cases} \tag{6}$$

where the switching function S is

$$S = -\frac{I_{\mathrm{sp}} \, g_0}{m} \lambda_v - \lambda_m \tag{7}$$

Singular arcs with $S = 0$ are not considered in this work. The motion of the spacecraft is determined by integrating the following dynamical equations (Zhang et al. 2015)

$$\dot{\boldsymbol{y}} = \boldsymbol{F}(\boldsymbol{y}) \Rightarrow \begin{cases} \dot{\boldsymbol{r}} = \boldsymbol{v} \\ \dot{\boldsymbol{v}} = \boldsymbol{g}(\boldsymbol{r}) + \boldsymbol{h}(\boldsymbol{v}) - u^* \dfrac{T_{\max}}{m} \dfrac{\boldsymbol{\lambda}_v}{\lambda_v} \\ \dot{m} = -u^* \dfrac{T_{\max}}{c} \\ \dot{\boldsymbol{\lambda}}_r = -A(\boldsymbol{r})^\top \boldsymbol{\lambda}_v \\ \dot{\boldsymbol{\lambda}}_v = -\boldsymbol{\lambda}_r - B(\boldsymbol{v})^\top \boldsymbol{\lambda}_v \\ \dot{\lambda}_m = -u^* \lambda_v \dfrac{T_{\max}}{m^2} \end{cases} \tag{8}$$

where $\boldsymbol{y} := [\boldsymbol{x}, \boldsymbol{\lambda}] \in \mathbb{R}^{14}$, $A(\boldsymbol{r}) := \partial \boldsymbol{g}(\boldsymbol{r}) / \partial \boldsymbol{r}$ and $B(\boldsymbol{v}) := \partial \boldsymbol{h}(\boldsymbol{v}) / \partial \boldsymbol{v}$.

Since the terminal mass is free and the augmented terminal cost does not explicitly depend on the mass, the transversality condition for the free terminal mass is

$$\lambda_m(t_f) = 0 \tag{9}$$

From Eq. (8), we have that $\dot{\lambda}_m \leq 0$. Then, $\lambda_m(t_f) = 0$ implies $\lambda_m(t) \geq 0$, thus $S < 0$ and $u^* = 1$ for the whole time-optimal trajectory. Also, the optimal thrust direction in Eq. (5) varies continuously. Therefore, the time-optimal problem considered in this work is unconstrained on the control.

The Hamiltonian function at the terminal time t_f satisfies

$$H = 0 \tag{10}$$

The following two categories of boundary conditions are discussed:

1. Fixed-point initial conditions and soft terminal conditions. In this case, t_i is fixed, and t_f is free. The fixed-point initial condition is

$$\boldsymbol{x}(t_i) = \boldsymbol{x}_i \tag{11}$$

and the soft terminal condition is

$$\hat{\boldsymbol{\phi}}(\boldsymbol{r}(t_f), \boldsymbol{v}(t_f)) = \boldsymbol{0} \in \mathbb{R}^k, \quad k < 6 \tag{12}$$

The corresponding transversality condition at t_f is

$$\boldsymbol{\lambda}^\top(t_f) - \boldsymbol{\chi}^\top \frac{\partial \hat{\boldsymbol{\phi}}}{\partial \boldsymbol{x}(t_f)} = \boldsymbol{0} \tag{13}$$

If the multiplier $\boldsymbol{\chi}$ can be eliminated by algebraic manipulations, the terminal conditions in Eqs. (12) and (13) are combined and denoted as

$$\boldsymbol{\phi}(\boldsymbol{y}(t_f)) = \boldsymbol{0} \in \mathbb{R}^6 \tag{14}$$

Remark 1 Let $\boldsymbol{\varphi}(t_f, t_i, [\boldsymbol{\lambda}_i, \boldsymbol{x}_i], T_{\max})$ be the solution of Eq. (8) integrated forward from t_i to t_f with the given initial conditions and $T_{\max}$, the time-optimal problem is to find the optimal $\boldsymbol{\xi}^* := [\boldsymbol{\lambda}_i^*, t_f^*] \in \mathbb{R}^8$ such that $\boldsymbol{y}_f^* := \boldsymbol{\varphi}(t_f^*, t_i, [\boldsymbol{\lambda}_i^*, \boldsymbol{x}_i], T_{\max})$ satisfies $\boldsymbol{\psi}(\boldsymbol{y}_f^*, T_{\max}) := [\boldsymbol{\phi}(\boldsymbol{y}_f^*), \lambda_m(t_f^*), H(\boldsymbol{y}_f^*)] = \boldsymbol{0}_{8\times 1}$.

2. Soft initial conditions and fixed-point terminal conditions. In this case, t_i is free, and t_f is fixed. The fixed-point terminal condition is

$$\boldsymbol{r}(t_f) = \boldsymbol{r}_f, \quad \boldsymbol{v}(t_f) = \boldsymbol{v}_f \tag{15}$$

and the soft initial condition is

$$\hat{\boldsymbol{\phi}}(\boldsymbol{r}(t_i), \boldsymbol{v}(t_i)) = \boldsymbol{0} \in \mathbb{R}^k, \quad k < 6 \tag{16}$$

The corresponding transversality condition at t_i is

$$\boldsymbol{\lambda}^{\top}(t_i) - \boldsymbol{\chi}^{\top}\frac{\partial \hat{\boldsymbol{\phi}}}{\partial \boldsymbol{x}(t_i)} = \mathbf{0} \tag{17}$$

Again, if the multipliers $\boldsymbol{\chi}$ can be eliminated by algebraic manipulations, the initial conditions in Eqs. (16) and (17) are combined and denoted as

$$\boldsymbol{\phi}(\boldsymbol{y}_i) = \mathbf{0} \in \mathbb{R}^6 \tag{18}$$

The mass of the spacecraft at t_i should satisfy

$$m(t_i) = m_i \tag{19}$$

where m_i is the specified initial mass of the spacecraft.

Remark 2 Let $\boldsymbol{\varphi}(t_i, t_f, [\boldsymbol{\lambda}_{rf}, \boldsymbol{\lambda}_{vf}, \lambda_{mf} = 0, \boldsymbol{r}_f, \boldsymbol{v}_f, m_f], T_{\max})$ be the solution of Eq. (8) integrated backward from t_f to t_i with the given terminal conditions and $T_{\max}$, the time-optimal problem is to find the optimal $\boldsymbol{\xi}^* := [\boldsymbol{\lambda}^*_{rf}, \boldsymbol{\lambda}^*_{vf}, m^*_f, t^*_f] \in \mathbb{R}^8$ such that $\boldsymbol{y}^*_f := [\boldsymbol{r}_f, \boldsymbol{v}_f, \boldsymbol{m}^*_f, \boldsymbol{\lambda}^*_{rf}, \boldsymbol{\lambda}^*_{vf}, 0]$ and $\boldsymbol{y}^*_i := \boldsymbol{\varphi}(t_i, t^*_f, \boldsymbol{y}^*_f, T_{\max})$ satisfy $\boldsymbol{\psi}(\boldsymbol{y}^*_f, \boldsymbol{y}^*_i) := [\boldsymbol{\phi}(\boldsymbol{y}^*_i), m(t^*_i) - m_i, H(\boldsymbol{y}^*_f)] = \mathbf{0}_{8\times 1}$.

Remark 3 The elimination of the multipliers $\boldsymbol{\chi}$ is not required for the presented method. This assumption is added to make the problem statement coincide with the simulation examples.

Remark 4 Cartesian coordinates are used mainly because: 1) they are conveniently used in the multi-body problem; 2) Reduced transversality conditions in Pan et al. (2013) allow tackling various orbital transfer problems as soft terminal conditions without the need to solve for the multipliers.

Remark 5 The backward integration is used in Remark 2, so initial conditions in Remark 2 act as terminal conditions in Remark 1. Thus, the problem statement in Remark 1 is used to depict the method in Sect. 3.

3 Thrust continuation method

3.1 Ill-conditioned homotopy path

Thrust continuation approaches the many-revolution, low-thrust solution starting from the few-revolution, high-thrust solution that is easier to find. Suppose the time-optimal solution $\boldsymbol{\lambda}^*_i$ and t^*_f with the given $T_{\max}$ is solved, the neighborhood optimal trajectory for the small thrust variation $T_{\max} + \mathrm{d}T_{\max}$ satisfies

$$\begin{aligned}&\boldsymbol{\psi}(\boldsymbol{y}_f(\boldsymbol{x}_i, \boldsymbol{\lambda}^*_i + \mathrm{d}\boldsymbol{\lambda}_i, T_{\max} + \mathrm{d}T_{\max}, t^*_f + \mathrm{d}t_f),\\ &\quad T_{\max} + \mathrm{d}T_{\max}) = \mathbf{0}\end{aligned} \tag{20}$$

Taking the differential of Eq. (20) yields

$$\begin{aligned}\mathrm{d}\boldsymbol{\psi} = &\frac{\partial \boldsymbol{\psi}}{\partial \boldsymbol{y}_f}\frac{\partial \boldsymbol{y}_f}{\partial \boldsymbol{\lambda}^*_i}\mathrm{d}\boldsymbol{\lambda}^*_i + \frac{\partial \boldsymbol{\psi}}{\partial \boldsymbol{y}_f}\dot{\boldsymbol{y}}_f \mathrm{d}t^*_f\\ &+ \left(\frac{\partial \boldsymbol{\psi}}{\partial \boldsymbol{y}_f}\frac{\partial \boldsymbol{y}_f}{\partial T_{\max}} + \frac{\partial \boldsymbol{\psi}}{\partial T_{\max}}\right)\mathrm{d}T_{\max} = \mathbf{0}\end{aligned} \tag{21}$$

Then, there exists

$$\begin{bmatrix}\dfrac{\partial \boldsymbol{\lambda}^*_i}{\partial T_{\max}}\\ \dfrac{\partial t^*_f}{\partial T_{\max}}\end{bmatrix} = -D^{-1}\boldsymbol{b} \tag{22}$$

where

$$\begin{aligned}D &= \left[\frac{\partial \boldsymbol{\psi}}{\partial \boldsymbol{y}_f}\frac{\partial \boldsymbol{y}_f}{\partial \boldsymbol{\lambda}^*_i}, \frac{\partial \boldsymbol{\psi}}{\partial \boldsymbol{y}_f}\dot{\boldsymbol{y}}_f\right],\\ \boldsymbol{b} &= \frac{\partial \boldsymbol{\psi}}{\partial \boldsymbol{y}_f}\frac{\partial \boldsymbol{y}_f}{\partial T_{\max}} + \frac{\partial \boldsymbol{\psi}}{\partial T_{\max}}\end{aligned} \tag{23}$$

and $\partial \boldsymbol{y}_f / \partial T_{\max}$ satisfies the following dynamical equations

$$\frac{\mathrm{d}}{\mathrm{d}t}\frac{\partial \boldsymbol{y}}{\partial T_{\max}} = \frac{\partial \boldsymbol{F}}{\partial \boldsymbol{y}}\frac{\partial \boldsymbol{y}}{\partial T_{\max}} + \frac{\partial \boldsymbol{F}}{\partial T_{\max}} \tag{24}$$

with the initial condition $\partial \boldsymbol{y}/\partial T_{\max}(t_i) = \mathbf{0}_{14\times 1}$.

From the implicit function theorem, the thrust continuation enables us to proceed by reducing $T_{\max}$ if the matrix D in Eq. (22) is regular. However, the right-hand side of Eq. (22) may go off to infinity when approaching a certain $T_{\max}$ value. At the same time, as shown in Fig. 1, it is possible that 1) the costate goes off to infinity as well; 2) the costate remains finite, and the corresponding termination point is called the limit point (Pan et al. 2016). Other types of singular points where homotopy path branches emanate will not be considered in this work.

A simple path-tracking method is to monotonously decrease $T_{\max}$ at each step. This method is easy to implement but lacks the capability to tackle homotopy paths in Fig. 1. PAM enables one to pass limit points by reversing the path direction, i.e., by increasing the thrust magnitude (Wang and

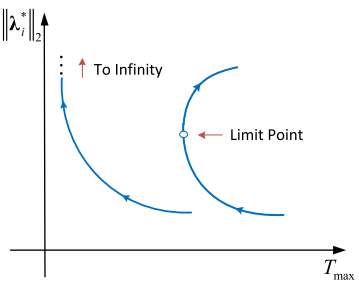

Fig. 1 Two types of ill-conditioned homotopy paths

Topputo 2022). However, another limit point should exist along the path to reverse the path again. Also, PAM fails for case 1. This work tackles issues of ill-conditioned homotopy paths by designing a second-layer continuation. As a result, it is sufficient to monotonously vary the homotopy parameter in the simulation studies.

3.2 Connection of solution curves

The two-layer thrust continuation method is shown in Fig. 2. Suppose that the solution curve α is traced by gradually reducing $T_{\max}$ until the continuation terminates at the solution $\boldsymbol{\xi}^*_{\alpha,f}$. Based on the fact that multiple solutions with the same $T_{\max}$ exist for the time-optimal orbital transfer problem (Caillau and Farrés 2016), the method searches the solution $\boldsymbol{\xi}^*_{\beta,0}$ from $\boldsymbol{\xi}^*_{\alpha,f}$ by solving a series of auxiliary problems. Then, the thrust continuation proceeds by tracking the solution curve β starting from the solution $\boldsymbol{\xi}^*_{\beta,0}$.

Figure 3 shows the process to find the solution $\boldsymbol{\xi}^*_{\beta,0}$ for fixed-point terminal conditions (Ferella 2016). The auxiliary orbit that frees the true anomaly of the terminal point is identified first. Starting from the solution $\boldsymbol{\xi}^*_{\alpha,f}$, a succession of auxiliary problems that aim to reach the new terminal point is solved, where the new terminal point is determined by the increased true anomaly. The solution $\boldsymbol{\xi}^*_{\beta,0}$ is found once the true anomaly increases by 2π, indicating that the solution $\boldsymbol{\xi}^*_{\beta,0}$ has one more revolution than the solution $\boldsymbol{\xi}^*_{\alpha,f}$. The stop condition when the solution $\boldsymbol{\xi}^*_{\beta,0}$ is reached is common for other transfer problems with fixed-point terminal constraints. One aim of our method design is to find the stop condition that can be commonly used for different soft terminal conditions and dynamics.

With reference to Fig. 4, the angle $\zeta(\boldsymbol{r})$ is introduced as a function of $\boldsymbol{r}$. The increment of the variable ζ represents the angle that the trajectory has swept through. Then, the number of revolutions of the trajectory is defined as

$$N_{\text{rev}} = \frac{\zeta_f - \zeta_i}{2\pi} \tag{25}$$

where ζ_i and ζ_f are values of ζ at the initial and terminal time. The solution corresponding to a larger value of

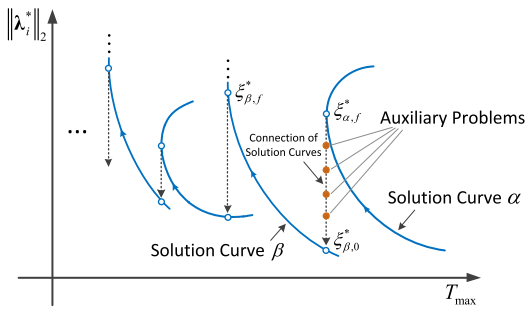

Fig. 2 Thrust continuation by switching from the solution curve α to β through solving a series of auxiliary problems

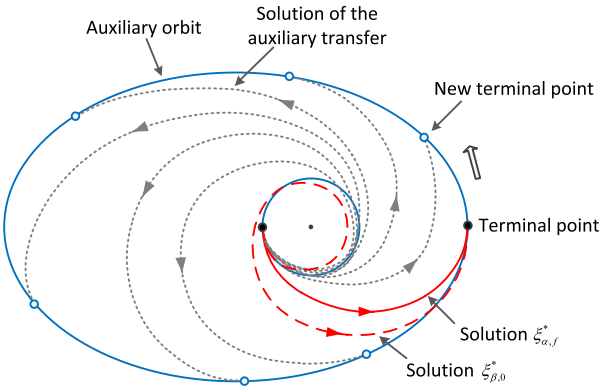

Fig. 3 Find $\boldsymbol{\xi}^*_{\beta,0}$ from $\boldsymbol{\xi}^*_{\alpha,f}$ for the fixed-point terminal conditions

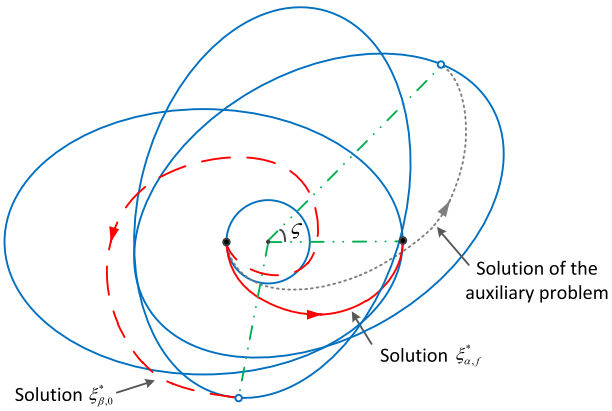

Fig. 4 Solution connection for soft terminal conditions

ζ_f involves more revolutions. Differently from the work in (Ferella 2016), the true anomaly is not employed since its dynamic equation involves control variables whereas $\dot{\zeta}$ does not. Also, the true anomaly is not conveniently used for multi-body dynamics, especially when the rotating frame is employed. The use of ζ is the foundation for the definition of the auxiliary problem in the following.

The state $\boldsymbol{x}$ is augmented by the variable ζ. The equations of augmented dynamics are

$$\frac{\mathrm{d}\hat{\boldsymbol{x}}}{\mathrm{d}t} = \boldsymbol{f}(\hat{\boldsymbol{x}}, u, \boldsymbol{\alpha}) \Rightarrow \begin{cases} \dot{\boldsymbol{r}} = \boldsymbol{v} \\ \dot{\boldsymbol{v}} = \boldsymbol{g}(\boldsymbol{r}) + \boldsymbol{h}(\boldsymbol{v}) + u\dfrac{T_{\max}}{m}\boldsymbol{\alpha} \\ \dot{m} = -u\dfrac{T_{\max}}{I_{\text{sp}}\, g_0} \\ \dot{\zeta} = \sigma(\boldsymbol{r}, \boldsymbol{v}) = \dfrac{\partial \zeta}{\partial \boldsymbol{r}}\boldsymbol{v} \end{cases} \tag{26}$$

where $\hat{\boldsymbol{x}} := [\boldsymbol{x}, \zeta]$ is the augmented state.

The corresponding augmented Hamiltonian function is

$$\begin{aligned}\hat{H} = 1 + \boldsymbol{\lambda}_r^\top \boldsymbol{v} + \boldsymbol{\lambda}_v^\top \left(\boldsymbol{g}(\boldsymbol{r}) + \boldsymbol{h}(\boldsymbol{v}) + u\frac{T_{\max}}{m}\boldsymbol{\alpha} \right) \\ - \lambda_m u \frac{T_{\max}}{I_{\mathrm{sp}} g_0} + \lambda_\zeta \sigma(\boldsymbol{r}, \boldsymbol{v})\end{aligned} \tag{27}$$

The $\boldsymbol{\alpha}^*$ and u^* are the same as Eqs. (5) and (6), since $\dot{\zeta}$ does not contain control variables. The motion of the spacecraft is determined by integrating the following augmented state-costate dynamics

$$\frac{\mathrm{d}\hat{\boldsymbol{y}}}{\mathrm{d}t} = \hat{\boldsymbol{F}}(\hat{\boldsymbol{y}}) \Rightarrow \begin{cases} \dot{\boldsymbol{r}} = \boldsymbol{v} \\ \dot{\boldsymbol{v}} = \boldsymbol{g}(\boldsymbol{r}) + \boldsymbol{h}(\boldsymbol{v}) + u\dfrac{T_{\max}}{m}\dfrac{\boldsymbol{\lambda}_v}{\lambda_v} \\ \dot{m} = -u\dfrac{T_{\max}}{I_{\mathrm{sp}}\, g_0} \\ \dot{\zeta} = \sigma(\boldsymbol{r}, \boldsymbol{v}) \\ \dot{\boldsymbol{\lambda}}_r = -A^\top \boldsymbol{\lambda}_v - \lambda_\zeta \left(\dfrac{\partial \sigma(\boldsymbol{r}, \boldsymbol{v})}{\partial \boldsymbol{r}} \right)^\top \\ \dot{\boldsymbol{\lambda}}_v = -\boldsymbol{\lambda}_r - B^\top \boldsymbol{\lambda}_v - \lambda_\zeta \left(\dfrac{\partial \sigma(\boldsymbol{r}, \boldsymbol{v})}{\partial \boldsymbol{v}} \right)^\top \\ \dot{\lambda}_m = -u\lambda_v \dfrac{T_{\max}}{m^2} \\ \dot{\lambda}_\zeta = 0 \end{cases} \tag{28}$$

where $\hat{\boldsymbol{y}} := [\hat{\boldsymbol{x}}, \hat{\boldsymbol{\lambda}}] \in \mathbb{R}^{16}$ and $\hat{\boldsymbol{\lambda}} := [\boldsymbol{\lambda}, \lambda_\zeta]$.

In Eq. (28), $\dot{\lambda}_\zeta = 0$ implies the value of λ_ζ is constant during the flight. It can be seen that the solution of the augmented problem is equivalent to the solution of the original problem if

$$\lambda_\zeta = 0 \tag{29}$$

Let $\hat{\boldsymbol{\varphi}}(t, t_i, [\hat{\boldsymbol{\lambda}}_i, \hat{\boldsymbol{x}}], T_{\max})$ be the solution integrating Eq. (28) from t_i to a general time t, the following two problems are defined:

Definition 1 (Problem $\mathtt{P}_{\mathrm{org}}$) Find the optimal $\hat{\boldsymbol{\lambda}}_i^*$ and t_f^* such that

$$\hat{\boldsymbol{\varphi}}(t_f^*, t_i, [\hat{\boldsymbol{\lambda}}_i^*, \hat{\boldsymbol{x}}_i], T_{\max}) \text{ satisfies } \begin{cases} \boldsymbol{\psi}(\boldsymbol{y}_f^*) = \boldsymbol{0} \\ \lambda_\zeta(t_f) = 0 \end{cases} \tag{30}$$

Definition 2 (Problem $\mathtt{P}_{\mathrm{aux}}$) Find the optimal $\hat{\boldsymbol{\lambda}}_i^*$ and t_f^* such that

$$\hat{\boldsymbol{\varphi}}(t_f^*, t_i, [\hat{\boldsymbol{\lambda}}_i^*, \hat{\boldsymbol{x}}_i], T_{\max}) \text{ satisfies } \begin{cases} \boldsymbol{\psi}(\boldsymbol{y}_f^*) = \boldsymbol{0} \\ \zeta(t_f) = \hat{\zeta} \end{cases} \tag{31}$$

where $\hat{\zeta}$ is a prescribed value.

Here, Problem $\mathtt{P}_{\mathrm{org}}$ is equivalent to the original problem as stated in Remark 1, while Problem $\mathtt{P}_{\mathrm{aux}}$ is the auxiliary problem. The solution of Problem $\mathtt{P}_{\mathrm{org}}$ is equivalent to the solution of Problem $\mathtt{P}_{\mathrm{aux}}$ if $\hat{\zeta}$ is set to the terminal value of ζ calculated from the solution of $\mathtt{P}_{\mathrm{org}}$. Besides, Problem $\mathtt{P}_{\mathrm{org}}$ offers a simple criterion to switch from $\mathtt{P}_{\mathrm{aux}}$ to $\mathtt{P}_{\mathrm{org}}$, i.e., $\lambda_\zeta(t_f) = 0$. Thus, the solution of Problem $\mathtt{P}_{\mathrm{aux}}$ is equivalent to the solution of Problem $\mathtt{P}_{\mathrm{org}}$ if $\lambda_\zeta(t_f) = 0$ is additionally satisfied. It is clear that the condition $\lambda_\zeta(t_f) = 0$ can be commonly applied to other orbital transfer problems with soft terminal conditions. In summary, the proposed simple method is effective because the solution switching between $\mathtt{P}_{\mathrm{org}}$ and $\mathtt{P}_{\mathrm{aux}}$ is smooth. Besides, the following assumption is required for its effectiveness.

Remark 6 It is assumed that all auxiliary problems can be solved.

The indirect method featuring analytic gradients is employed to solve the time-optimal problem (Zhang et al. 2015). The gradients are computed through the state transition matrix (STM), subject to

$$\dot{\Phi}(t_i, t) = D_{\boldsymbol{y}} \hat{\boldsymbol{F}} \Phi(t_i, t) \quad \Phi(t_i, t_i) = \boldsymbol{I}_{16\times 16} \tag{32}$$

where $D_{\boldsymbol{y}} \hat{\boldsymbol{F}}$ is the jacobian matrix of $\hat{\boldsymbol{F}}(\hat{\boldsymbol{y}})$ w.r.t. $\hat{\boldsymbol{y}}$. Let $\boldsymbol{z} = [\hat{\boldsymbol{y}}, \mathrm{vec}(\Phi)]$ be a vector containing $\hat{\boldsymbol{y}}$ and columns of Φ. There exists

$$\dot{\boldsymbol{z}} = \boldsymbol{G}(\boldsymbol{z}) \Rightarrow \begin{pmatrix} \dot{\hat{\boldsymbol{y}}} \\ \mathrm{vec}(\dot{\Phi}) \end{pmatrix} = \begin{pmatrix} \hat{\boldsymbol{F}}(\hat{\boldsymbol{y}}) \\ \mathrm{vec}(D_{\boldsymbol{y}} \hat{\boldsymbol{F}} \Phi) \end{pmatrix} \tag{33}$$

The dynamical equations are integrated using variable–step seventh/eighth Runge–Kutta integration scheme (Zhang et al. 2015).

4 Numerical simulations

In this section, simulation examples under two- or three-body dynamics are conducted under the Windows 10 system with MATLAB R2019a.

4.1 GTO to GEO transfers

The two-body dynamics with Cartesian coordinates are employed, i.e.,

$$\boldsymbol{g}(\boldsymbol{r}) = -\mu_E \frac{\boldsymbol{r}}{r^3}, \quad \boldsymbol{h}(\boldsymbol{v}) = \boldsymbol{0} \tag{34}$$

where μ_E is the Earth gravitational parameter (see Table 1).

The variable ζ is defined as

$$\zeta = \arctan \frac{y}{x} \tag{35}$$

Table 1 Physical parameters

Physical constant	Value
Mass parameter, μ_E	398,600.4418 km^3/s^2
Gravitational field, g_0	9.80665 m/s^2
Length unit, LU	6378.137 km
Time unit, TU	806.8111 s
Velocity unit, VU	7.9054 km/s
Mass unit, MU	1500 kg
Specific Impulse, I_{sp}	1994.75 s

Table 2 Orbital elements of GTO and GEO

Orbit	a (km)	e	i (deg)	Ω (deg)	w (deg)	θ (deg)
GTO	26,571.43	0.75	7.004	0	0	180
GEO	42,165	0	0	free	free	free

with the following dynamic equation

$$\dot{\zeta} = \sigma(\boldsymbol{r}, \boldsymbol{v}) = \frac{x v_y - y v_x}{x^2 + y^2} \tag{36}$$

The scaling units and spacecraft parameters are listed in Table 1, where the initial spacecraft mass is equivalent to the mass unit. Time-optimal transfers from GTO to GEO extracted from Caillau et al. (2003) are solved. The orbital elements of GTO and GEO are shown in Table 2 where the eccentricity e and the inclination i of GEO are set to 0, and the right ascension of the ascending node Ω, the argument of perigee ω, the true anomaly θ of GEO are free. The corresponding terminal conditions are (Pan et al. 2013)

$$\boldsymbol{\phi}(\hat{\boldsymbol{y}}_f) = \begin{cases} \boldsymbol{h}_f^\top \boldsymbol{h}_f - h^2 \\ \frac{1}{2}\boldsymbol{v}_f^\top \boldsymbol{v}_f - \frac{1}{r_f} + \frac{\mu}{2a} \\ \boldsymbol{I}_z^\top \boldsymbol{h}_f - h\cos i \\ \left(\boldsymbol{\lambda}_{rf} \times \boldsymbol{r}_f + \boldsymbol{\lambda}_{vf} \times \boldsymbol{v}_f\right)^\top \boldsymbol{h}_f \\ \left(\boldsymbol{\lambda}_{rf} \times \boldsymbol{r}_f + \boldsymbol{\lambda}_{vf} \times \boldsymbol{v}_f\right)^\top \boldsymbol{I}_z \\ \boldsymbol{\lambda}_{rf}^\top \boldsymbol{v}_f - \frac{\mu}{r_f^3} \boldsymbol{\lambda}_{vf}^\top \boldsymbol{r}_f \end{cases} \tag{37}$$

where $\boldsymbol{I}_z = [0, 0, 1]^\top$ and $h = \sqrt{\mu_E a(1-e^2)}$.

The thrust continuation starts from the time-optimal transfer with $T_{\max} = 60$ N, and corresponding optimal solution is $\boldsymbol{\lambda}_{ri}^* = [-2.206184, -1.192697, -0.401076]$, $\boldsymbol{\lambda}_{vi}^* = [-47.309921, 48.309300, -21.856674]$, $\lambda_{mi} = 29.145137$, $t_f^* = 14.80$ hours. The optimal trajectory encompasses only 1.05 revolutions; see case A in Table 3.

The procedure of thrust continuation is illustrated in Fig. 5, including the variations of the norm of optimal initial costate and the optimal transfer time with respect to $T_{\max}$. In Caillau et al. (2003), it was stated that the lowest thrust solvable when using Cartesian coordinates is 0.7 N. Our simulations show that the proposed method can reach $T_{\max} \leq 0.7$. From Fig. 5a, it can be seen that the frequency of the curve connection increases as $T_{\max}$ decreases. Figure 5b shows that the optimal transfer time t_f^* grows rapidly as $T_{\max}$ reduces. The zoom-in curve of Fig. 5b shows that t_f^* is not smoothly varied. The overview of sample solutions for different thrust levels is provided in Table 3, including the optimal transfer time, final mass, and orbital revolutions. It can be seen that the number of revolutions increases drastically as $T_{\max}$ reduces. The time-optimal trajectories, corresponding variations of u, S, m, and a, e, i for sample solutions A-D in Fig. 5a are shown in Fig. 6. It can be seen that as the number of revolutions increases, the evolution of a, e, and i becomes steady.

Table 3 Summary of solution points A-H

Case	$T_{\max}$ (N)	Transfer time (hours)	Final mass (kg)	N_{rev}
A	60	14.80	1336.58	1.05
B	12	70.19	1344.98	3.57
B1	12	70.25	1344.86	4.15
C	3	283.33	1343.58	14.66
C1	3	281.97	1344.32	15.16
C2	3	285.77	1342.23	15.84
D	0.5	1708.52	1342.79	87.73

Time-optimal solutions shown in Fig. 5a only represent one local solution for a given $T_{\max}$. The proposed method enables searching for other solutions by increasing or decreasing ζ. Figure 7 shows the multiple solutions for $T_{\max} = 12$ N and $T_{\max} = 3$ N. It is interesting to notice that t_f^* of local solutions is not monotonous with respect to N_{rev}. Also, the norm of costate increases as the revolution decreases, and the minimum-revolution solution has the largest norm of costate. In Fig. 7a, solution B1 is consistent with the time-optimal solution obtained in Caillau et al. (2003), which takes slightly longer time than solution B to reach GEO. Also, solution B is the solution with the fewest revolutions and shortest transfer time that can be obtained. The time-optimal trajectory for solution B1 is illustrated in Fig. 8a. In Fig. 7b, solution C2 is consistent with the solution obtained in Caillau et al. (2003) with the transfer time of 285.77 h, whereas only 283.33 h is required for solution C with the fewest revolutions. Moreover, solution C1 with the fewest transfer time 281.97 h is found. It indicates that the solution with minimum revolutions may not correspond to the one with globally minimum transfer time. This situation is more likely to exist for the optimal trajectory with soft terminal conditions where neighborhood solutions are close, i.e., the difference on the sweeping angle between neighborhood solutions is less than 2π. The time-optimal trajectory

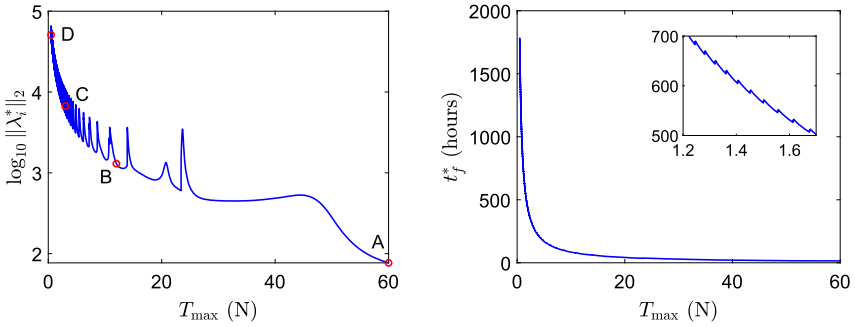

(a) Variations of $\|\boldsymbol{\lambda}_i^*\|_2$. (b) Variations of t_f^*.

Fig. 5 Variations of the norm of optimal initial costate $\|\boldsymbol{\lambda}_i^*\|_2$ and the optimal transfer time t_f^* w.r.t. $T_{\max}$

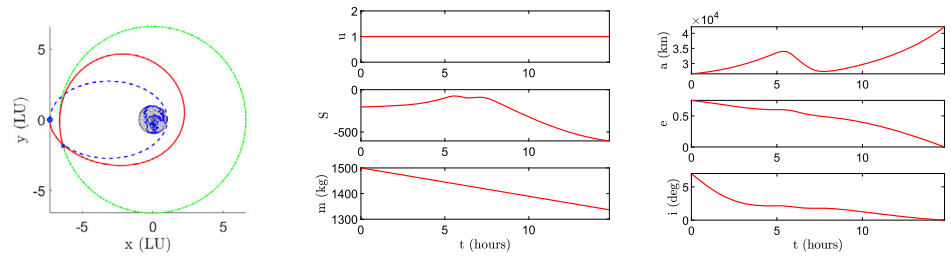

(a) Time-optimal solution with $T_{\max} = 60$N (Point A in Fig. 5a).

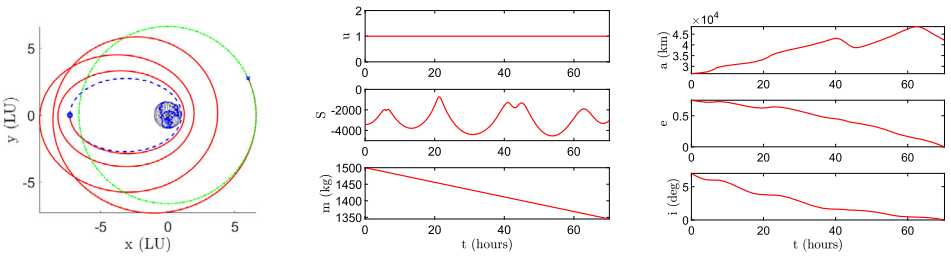

(b) Time-optimal solution with $T_{\max} = 12$N (Point B in Fig. 5a).

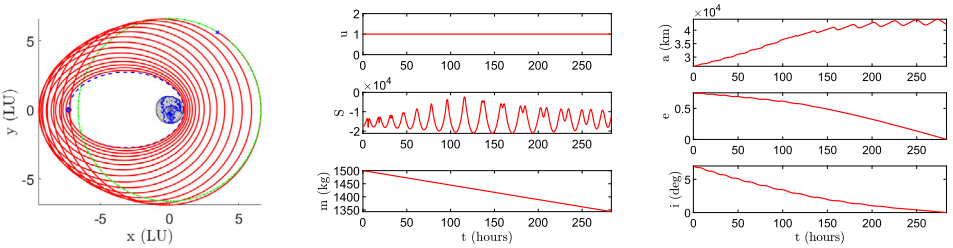

(c) Time-optimal solution with $T_{\max} = 3$N (Point C in Fig. 5a).

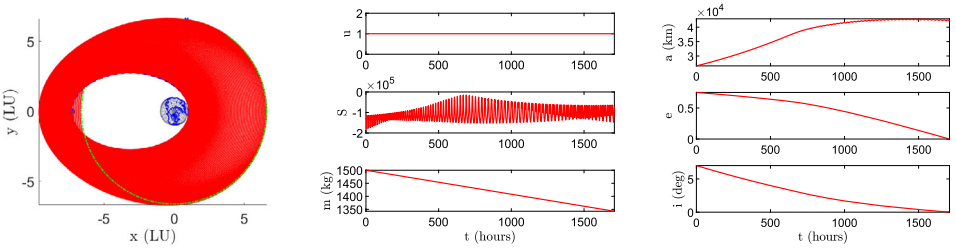

(d) Time-optimal solution with $T_{\max} = 0.5$N (Point D in Fig. 5a).

Fig. 6 Sample solutions A-D in Fig. 5a. Blue dashed line: GTO; green line: GEO. 'o': initial point; 'x': terminal point

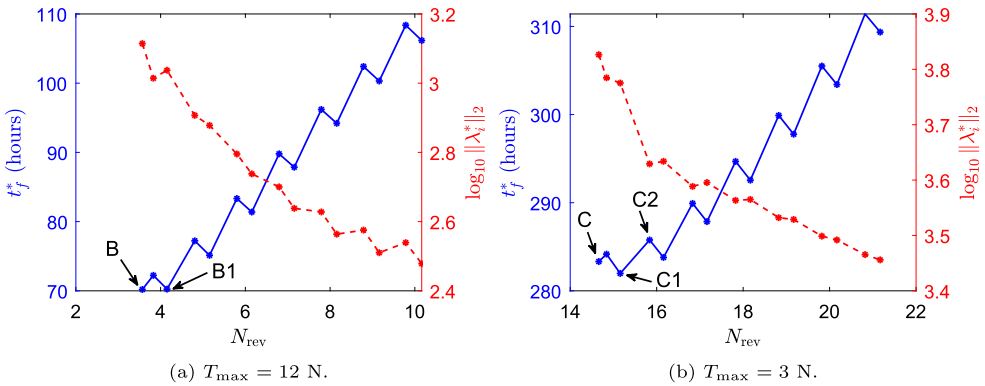

(a) $T_{\max} = 12$ N. (b) $T_{\max} = 3$ N.

Fig. 7 Multiple local solutions (labeled as dots) for $T_{\max} = 12$ N and $T_{\max} = 3$ N

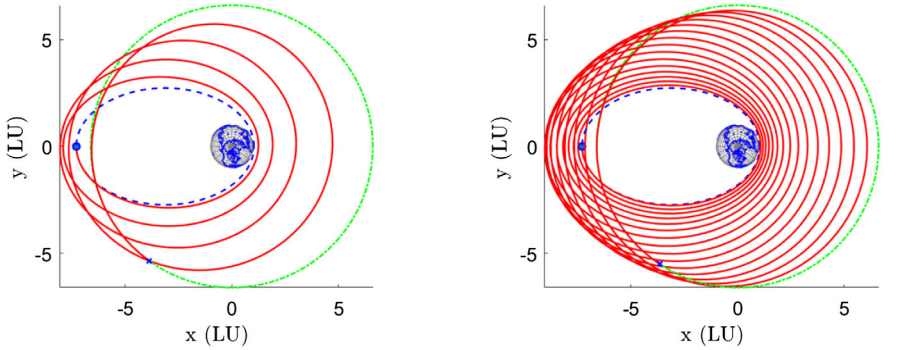

(a) Time-optimal trajectory of the solution B1 (b) Time-optimal trajectory of the solution C1

Fig. 8 Time-optimal trajectories for solutions B1 and C1 in Fig. 7. Blue dashed line: GTO; green line: GEO

for solution C1 is shown in Fig. 8b. Notice that the obtained solutions on the continuation path are not guaranteed to be always close to the globally minimum-time trajectory theoretically. The failed continuation point indicates that the optimal trajectory with the corresponding thrust level requires more revolutions to complete the transfer. The proposed algorithm then searches for the first locally optimal trajectory by sweeping ζ, and then executes the continuation from this solution. Therefore, the obtained solutions are at least close to the minimum-revolution trajectory.

4.2 GTO to EIGSO transfers

Time-optimal GTO-EIGSO trajectories are solved, where the semi-major axis a of EIGSO is the same as GEO in Table 2, e and i of EIGSO are specified by non-zero values, and Ω, ω, θ are free. The terminal conditions correspond to Eq. (37). In the following, i_f and e_f are denoted as the terminal i and e of EIGSO. Starting from the time-optimal GTO-GEO solution with $T_{\max} = 60$ N, the continuations on i_f and e_f are performed first to find solutions with $T_{\max} = 60$ N for the given i_f and e_f below.

With reference to Fig. 9, variations of $t_f^* \times T_{\max}$ with respect to the thrust level for i_f ranging from 5 deg to 50 deg and $e_f = 0.1$ are illustrated. It can be seen that the values of $t_f^* \times T_{\max}$ oscillate for large $T_{\max}$, then tend to be nearly constant as $T_{\max}$ reduces. The conservation of $t_f^* \times T_{\max}$ has

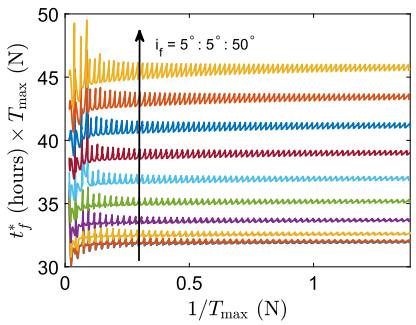

Fig. 9 Variation of $t_f^*(hours) \times T_{\max}(N)$ with $e_f = 0.1$ for various i_f

been shown for GTO-GEO transfers in Caillau et al. (2003). Our work shows that the conservation of $t_f^* \times T_{\max}$ exists for general orbital transfers. The constant is further estimated as the averaged value of t_f^* (hours) $\times T_{\max}$ (N) with $1/T_{\max}$ (N) ≥ 1 in Fig. 9, labeled as C.

To further study how the conservation C varies as i_f and e_f vary, simulations for various combinations of i_f and e_f are carried out. With reference to Fig. 10a, the variations of C for i_f ranging from 0° to 50° and $e_f = 0.1, 0.2, 0.3$ are illustrated. Let Δi and Δe be the absolute value of the difference of i and e between EIGSO and GTO, respectively. It can be seen from Fig. 10a that the fuel cost is the least for the planar transfer, and increases monotonously as Δi increases. In Fig. 10b, the variations of C for e_f ranging

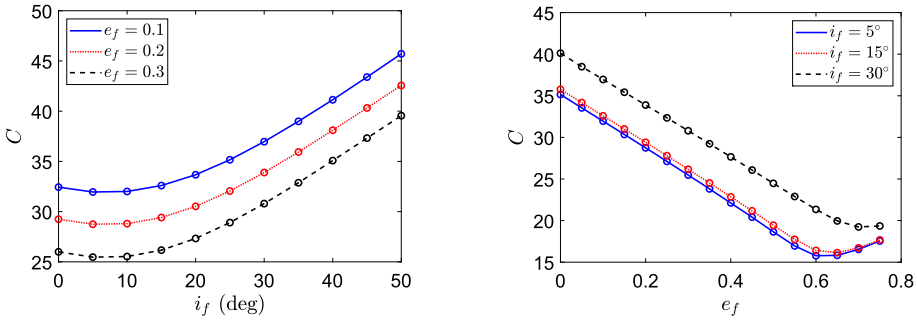

Fig. 10 Variation of C (the averaged value of $t_f^*\ (hours) \times T_{\max}\ (N)$)

(a) For varying i_f. (b) For varying e_f.

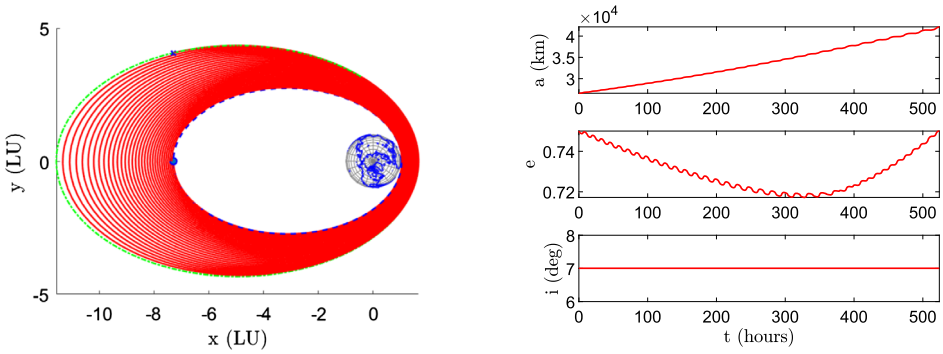

Fig. 11 Sample solution for the GTO to EIGSO transfer with $\Delta i = 0°$, $\Delta e = 0$ and $T_{\max} = 0.8$ N

(a) Optimal trajectory. (b) Optimal variations of a, e and i.

from 0 to 0.75 and $i_f = 5°, 15°, 30°$ are illustrated. It can be seen that the minimum fuel cost does not occur where $\Delta e = 0$. For the case $i_f = 5°$, as Δe increases, the value of C decreases first, then it increases almost linearly when Δe is higher than around 0.15. A sample solution with $\Delta i = 0$, $\Delta e = 0$, and $T_{\max} = 0.8$ N is shown in Fig. 11. It can be seen that i is constant while e is varying during the transfer. Therefore, the behaviors of e and i are different. It is noticed that the conservation of the product and its linear relationship with eccentricity apply to optimal trajectories with the low thrust. From the viewpoint of the averaging, the effect of changing the orbital elements (except true anomaly) over one revolution for the low thrust is small. The evolution of the trajectory is mainly dominated by the secular variation of the orbital elements, which is insensitive to the selection of the initial point.

4.3 GTO to Halo orbit transfers

To further verify the effectiveness of the presented method for multi-body dynamics, the time-optimal transfers from GTO to the Halo orbit are solved. The CRTBP dynamics under a rotating frame is employed, i.e.,

$$\boldsymbol{g}(\boldsymbol{r}) = \begin{bmatrix} x - (1-\mu)(x+\mu)/r_1^3 - \mu(x+\mu-1)/r_2^3 \\ y - (1-\mu)/r_1^3 - \mu y/r_2^3 \\ -(1-\mu)z/r_1^3 - \mu z/r_2^3 \end{bmatrix},$$

$$\boldsymbol{h}(\boldsymbol{v}) = \begin{bmatrix} 2v_y \\ -2v_y \\ 0 \end{bmatrix} \tag{38}$$

where $r_1 = ((x+\mu)^2 + y^2 + z^2)^{1/2}$, $r_2 = ((x-1+\mu)^2 + y^2 + z^2)^{1/2}$, and $\mu = m_2/(m_1+m_2)$ is the mass parameter, m_1 and m_2 are the mass of the Earth and the Moon, respectively.

Since the major part of the trajectory is around the Earth, the variable ζ is defined as

$$\zeta = \arctan \frac{y}{x+\mu} \tag{39}$$

with the following dynamics

$$\dot{\zeta} = \sigma(\boldsymbol{r}, \boldsymbol{v}) = \frac{(x+\mu)v_y - y v_x}{(x+\mu)^2 + y^2} \tag{40}$$

The perigee and apogee attitudes of the planar GTO and the fixed point of Halo orbit from Zhang et al. (2015) are used to construct the boundary conditions. Differently from Zhang et al. (2015) where the transfer begins at the perigee of the specified GTO, the longitude of GTO's perigee is free in our simulations, which is also studied in Pan et al. (2020). Scaling units, spacecraft parameters, perigee, and apogee of GTO are summarized in Table 4. The backward integration is executed with the shooting problem stated in Remark 2.

Table 4 Physical constants

Physical constant	Value
Mass parameter, μ	0.0121506683
Length unit, LU	384405 km
Time unit, TU	3.751977×10^5 s
Velocity unit, VU	1.024540 km/s
Mass unit, MU	1500 kg
Specific Impulse, I_{sp}	3000 s
Terminal position, LU	[0.823385182067; 0; −0.022277556273]
Terminal velocity, VU	[0; 0.134184170262; 0]
GTO perigee, km	400
GTO apoapsis, km	35864

The conditions at the perigee are

$$\boldsymbol{\phi}(\hat{\mathbf{y}}_i) = \begin{cases} \frac{1}{2}\left((x+\mu)^2 + y^2 - r_{\text{gto}}^2\right) \\ \frac{1}{2}\left((v_x - y)^2 + (v_y + x + \mu)^2 - v_{\text{gto}}^2\right) \\ (x+\mu)(v_x - y) + y(v_y + x + \mu) \\ (x+\mu)\lambda_y - y\lambda_x + v_x\lambda_{vy} - v_y\lambda_{vx} \\ z \\ v_z \end{cases} \tag{41}$$

where $r_{\text{gto}} = 0.0176328013$ LU and $v_{\text{gto}} = 9.8261812084$ VU are magnitudes of radius and velocity of the spacecraft at the GTO's perigee. The thrust continuation starts from the time-optimal transfer with $T_{\max} = 100$N. The corresponding optimal solution is $\boldsymbol{\lambda}_{rf}^* = [-0.230307, 0.004154, 0.007510]$, $\boldsymbol{\lambda}_{vf}^* = [0.029780, -0.004956, -0.001141]$, $t_f^* = 1.355$ days and $m_f^* = 1102.7$ kg. The thrust continuation is illustrated in Fig. 12, where the continuation jumps between long and short curves that are categorized based on the curve length. Solutions with shorter transfer time than solutions on the short curve can be obtained when tracking backward the solutions on the long curve. Thus, solutions on the long curve are desired, and the value of $t_f^* \times T_{\max}$ on long curves tends to be constant as $T_{\max}$ reduces. Sample solutions for $T_{\max} = 3$ N and $T_{\max} = 0.6$ N are provided in Table 5. The corresponding time-optimal trajectories and variations of S and m are shown in Fig. 13. Compared to the results in (Pan et al. 2020), the fuel consumption and transfer time are slightly different, because the approximated velocity constraint is used for the conditions of GTO in (Pan et al. 2020). Solutions obtained by this work and the work in (Pan et al. 2020) are better than the those in Zhang et al. (2015) which is 21.1363 days for 3 N and 87.6674 days for 0.6 N.

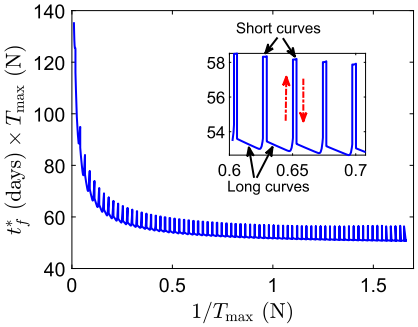

Fig. 12 Variations of t_f (days) $\times$ $T_{\max}$(N) with respect to $1/T_{\max}$(N)

Table 5 Summary of solution for $T_{\max} = 3$ N and 12 N

$T_{\max}$ (N)	Transfer time (days)	Final mass (kg)	N_{rev}
3	18.718	1335.09	13.91
0.6	84.713	1350.73	68.56

5 Conclusion

Thrust continuation is a natural way to solve low-thrust many-revolution time-optimal trajectories. This work addresses the ill-conditioned homotopy path in finding time-optimal trajectories with soft terminal conditions. A two-layer thrust continuation method is presented, where the second layer is designed to connect solutions with the same thrust level but different revolutions. The stop condition when searching for neighborhood solutions can be commonly used for different transfer problems. The effectiveness of the presented method has been validated by extensive simulations of time-optimal transfers under two- or three-body dynamics. The time-optimal solution on the obtained thrust continuation path is close or equivalent to the minimum-revolution time-optimal solution.

Numerical evidence reveals that: 1) the minimum-revolution solution may not coincide with the globally minimum-time solution; 2) The optimal trajectory with the same eccentricity at the boundary may require longer transfer time than the one with different eccentricity at the boundary; 3) the near conservation of the product between the time of flight and the thrust level exists for more general orbital transfers. The linear variation of this quantity with the eccentricity is demonstrated when the difference in eccentricity between the initial and terminal orbits is large enough.

The conclusions obtained in this work apply to the time-optimal trajectories that are unconstrained on the control. Future work will extend the developed method to tackle the time-optimal trajectories with thrust direction constraints, and the hybrid index that combines the transfer time and the fuel cost. For the latter problem, the optimal control exhibits the bang-bang control, and the strategy that tackles the continuation failure when the optimal trajectory adds or

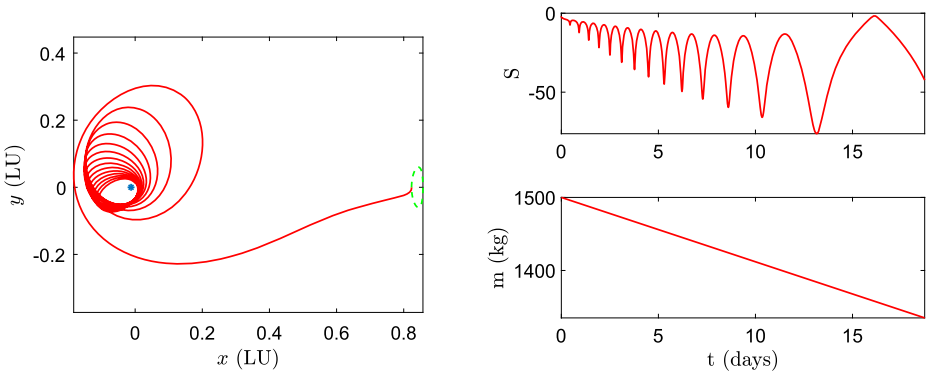

(a) Time-optimal solution with $T_{\max} = 3$N.

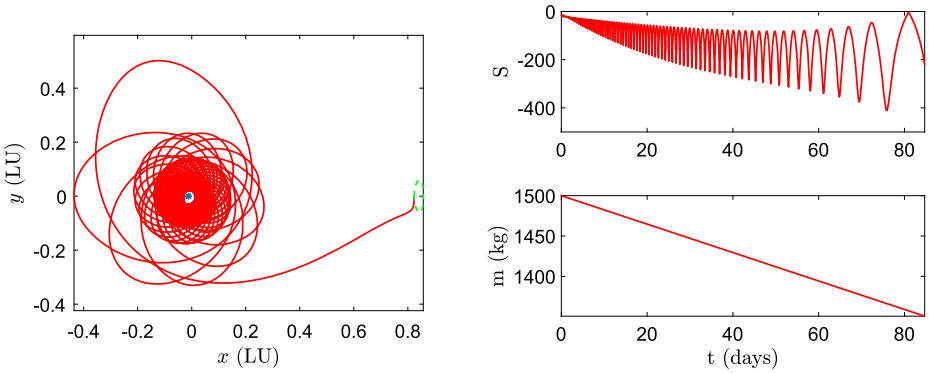

(b) Time-optimal solution with $T_{\max} = 0.6$N.

Fig. 13 Sample solutions. Green dashed line: Halo orbit

removes the thrust or coast arcs is required. Besides, future work will include the theoretical study to explain the variation of the conservation with eccentricity.

Acknowledgements The authors would like to thank Prof. Hanlun Lei for the fruitful discussions. Y.W. thanks the support from China Postdoctoral Science Foundation (No. 2023M741638). X.H. thanks the support from National Natural Science Foundation of China (No. 12233003).

Author contributions Methodology: Y.W.; Software: Y.W. and F.T.; Writing - original draft preparation: Y.W. and F.T.; Writing - review and editing: X.H. and F.T.; Simulation analysis: Y.W. and X.H.

Data Availability No datasets were generated or analysed during the current study.

Declarations

Competing interests The authors declare no competing interests.

References

Allgower, E., Georg, K.: Introduction to Numerical Continuation Methods. SIAM, Philadelphia (2003). https://doi.org/10.1137/1.9780898719154

Aziz, J., Parker, J., Scheeres, D., Englander, J.: Low-thrust many-revolution trajectory optimization via differential dynamic programming and a sundman transformation. J. Astronaut. Sci. **65**(2), 205–228 (2018). https://doi.org/10.1007/s40295-017-0122-8

Bertrand, R., Epenoy, R.: New smoothing techniques for solving bang–bang optimal control problems–numerical results and statistical interpretation. Optim. Control Appl. Methods **23**(4), 171–197 (2002). https://doi.org/10.1002/oca.709

Bonnard, B., Caillau, J.-B.: Geodesic flow of the averaged controlled Kepler equation. Forum Math. **21**(5), 797–814 (2009). https://doi.org/10.1515/FORUM.2009.038

Bryson, A., Ho, Y.-C.: Applied Optimal Control: Optimization, Estimation and Control. Taylor & Francis, New York (1975). https://doi.org/10.1109/TSMC.1979.4310229

Caillau, J.-B., Farrés, A.: On Local Optima in Minimum Time Control of the Restricted Three-Body Problem pp. 209–302. Springer, Cham (2016). https://doi.org/10.1007/978-3-319-27464-5_7

Caillau, J.-B., Gergaud, J., Noailles, J.: 3D geosynchronous transfer of a satellite: continuation on the thrust. J. Optim. Theory Appl. **118**(3), 541–565 (2003). https://doi.org/10.1023/B:JOTA.0000004870.74778.ae

Chi, Z., Yang, H., Chen, S., Li, J.: Homotopy method for optimization of variable-specific-impulse low-thrust trajectories. Astrophys. Space Sci. **362**(216), 1–13 (2017). https://doi.org/10.1007/s10509-017-3196-7

Conway, B.: A survey of methods available for the numerical optimization of continuous dynamic systems. J. Optim. Theory Appl. **152**(2), 271–306 (2012). https://doi.org/10.1007/s10957-011-9918-z

Coverstone-Carroll, V., Hartmann, J., Mason, W.: Optimal multi-objective low-thrust spacecraft trajectories. Comput. Methods Appl. Mech. Eng. **186**(2), 387–402 (2000). https://doi.org/10.1016/S0045-7825(99)00393-X

Ferella, L.: Indirect optimization of long-duration, multi-spiral low-thrust transfers with homotopy. Master's thesis, Politecnico di Milano (2016). https://www.politesi.polimi.it/handle/10589/123578

Li, T., Wang, Z., Zhang, Y.: A homotopy approach connecting time-optimal with fuel-optimal trajectories. Astrophys. Space Sci. **366**(11), 1–9 (2021). https://doi.org/10.1007/s10509-020-03890-7

Niccolai, L.: Optimal deep-space heliocentric transfers with an electric sail and an electric thruster. Adv. Space Res. **73**(1), 85–94 (2024). https://doi.org/10.1016/j.asr.2023.08.047

Pan, B., Chen, Z., Lu, P., Gao, B.: Reduced transversality conditions in optimal space trajectories. J. Guid. Control Dyn. **36**(5), 1289–1300 (2013). https://doi.org/10.2514/1.60181

Pan, B., Lu, P., Pan, X., Ma, Y.: Double-homotopy method for solving optimal control problems. J. Guid. Control Dyn. **39**(8), 1706–1720 (2016). https://doi.org/10.2514/1.G001553

Pan, B., Pan, X., Zhang, S.: A new probability-one homotopy method for solving minimum-time low-thrust orbital transfer problems. Astrophys. Space Sci. **363**(198), 1–12 (2018). https://doi.org/10.1007/s10509-018-3420-0

Pan, X., Pan, B., Li, Z.: Bounding homotopy method for minimum-time low-thrust transfer in the circular restricted three-body problem. J. Astronaut. Sci. **67**, 1220–1248 (2020). https://doi.org/10.1007/s40295-020-00213-4

Taheri, E.: Optimization of many-revolution minimum-time low-thrust trajectories using sundman transformation. In: AIAA Scitech 2021 Forum, p. 1343 (2021). https://doi.org/10.2514/6.2021-1343

Topputo, F., Zhang, C.: Survey of direct transcription for low-thrust space trajectory optimization with applications. Abstr. Appl. Anal. **2014**, Article ID 851720 (2014). https://doi.org/10.1155/2014/851720

Wang, Y., Topputo, F.: A TFC-based homotopy continuation algorithm with application to dynamics and control problems. J. Comput. Appl. Math. **401**, 113777 (2022). https://doi.org/10.1016/j.cam.2021.113777

Wang, Y., Topputo, F.: Indirect optimization of fuel-optimal many-revolution low-thrust transfers with eclipses. IEEE Trans. Aerosp. Electron. Syst. **59**(1), 39–51 (2023). https://doi.org/10.1109/TAES.2022.3189330

Yue, X., Yang, Y., Geng, Z.: Indirect optimization for finite-thrust time-optimal orbital maneuver. J. Guid. Control Dyn. **33**(2), 628–634 (2010). https://doi.org/10.2514/1.44885

Zhang, C., Topputo, F., Bernelli-Zazzera, F., Zhao, Y.: Low-thrust minimum-fuel optimization in the circular restricted three-body problem. J. Guid. Control Dyn. **38**(8), 1501–1510 (2015). https://doi.org/10.2514/1.G001080

Zhang, J., Xiao, Q., Li, L.: Solution space exploration of low-thrust minimum-time trajectory optimization by combining two homotopies. Automatica **148**, 110798 (2023). https://doi.org/10.1016/j.automatica.2022.110798